Construction and Building Materials 24 (2010) 2011–2021

Contents lists available at ScienceDirect

Construction and Building Materials

journal homepage: www.elsevier.com/locate/conbuildmat

# Analysis of strength development in cement-stabilized silty clay from microstructural considerations

Suksun Horpibulsuk [a,*], Runglawan Rachan [b], Avirut Chinkulkijniwat [a], Yuttana Raksachon [c], Apichat Suddeepong [c]

[a] Construction Technology Research Unit, School of Civil Engineering, Suranaree University of Technology, 111 University Avenue, Muang District, Nakhon Ratchasima 30000, Thailand
[b] Department of Civil Engineering, Mahanakorn University of Technology, 51 Cheum-Sampan Rd., Nong Chok, Bangkok 10530, Thailand
[c] School of Civil Engineering, Suranaree University of Technology, 111 University Avenue, Muang District, Nakhon Ratchasima 30000, Thailand

ARTICLE INFO

*Article history:*
Received 11 November 2009
Received in revised form 15 January 2010
Accepted 25 March 2010
Available online 27 April 2010

*Keywords:*
Cement-stabilized silty clay
Cementation
Fabric
Microstructure
Pore size distribution
Scanning electron microscope
Strength
Thermal gravity analysis

ABSTRACT

This paper analyzes the strength development in cement-stabilized silty clay based on microstructural considerations. A qualitative and quantitative study on the microstructure is carried out using a scanning electron microscope, mercury intrusion pore size distribution measurements, and thermal gravity analysis. Three influential factors in this investigation are water content, curing time, and cement content. Cement stabilization improves the soil structure by increasing inter-cluster cementation bonding and reducing the pore space. As the cement content increases for a given water content, three zones of improvement are observed: active, inert and deterioration zones. The active zone is the most effective for stabilization where the cementitious products increase with cement content and fill the pore space. In the active zone, the effective mixing state is achieved when the water content is 1.2 times the optimum water content. In this state, the strength is the greatest because of the highest quantity of cementitious products. In the short stabilization period, the volume of large pores (larger than 0.1 μm) increases because of the input of coarser particles (unhydrated cement particles) while the volume of small pores (smaller than 0.1 μm) decreases because of the solidification of the cement gel (hydrated cement). With time, the large pores are filled with the cementitious products; thus, the small pore volume increases, and the total pore volume decreases. This causes the strength development over time.



## 1. Introduction

Soil in northeast Thailand generally consists of two layers. The upper layer (varying from 0 to 3 m thickness) is wind-blown and has been deposited over several decades. It is clayey sand or silty clay with low to moderate strength ($12 < N < 20$, where $N$ is the standard penetration number). This upper soil is problematic because it is sensitive to changes in water content [1]. Its collapse behavior as a result of wetting is illustrated by Kohgo et al. [2]; and Kohgo and Horpibulsuk [3]. The lower layer is residual soil that is weathered from claystone and consists of clay, silt, and sand [4]. It possesses very high strength (generally $N > 30$) and very low compressibility. One of the most common soil improvement techniques for upper soil is to compact the in situ soil (in relatively a dry state) mixed with cement slurry. This technique is economical because cement is readily available at a reasonable cost in Thailand. Moreover, adequate strength can be achieved in a short time.

Stabilization begins by mixing the soil in a relatively dry state with cement and water specified for compaction. The soil, in the presence of moisture and a cementing agent becomes a modified soil, i.e., particles group together because of physical–chemical interactions among soil, cement and water. Because this occurs at the particle level, it is not possible to get a homogeneous mass with the desired strength. Compaction is needed to make soil particles slip over each other and move into a densely packed state. In this state, the soil particles can be welded by chemical (cementation) bonds and become an engineering material.

The effects of some influential factors, i.e., water content, cement content, curing time, and compaction energy on the engineering characteristics of cement-stabilized soils have been extensively researched [5–20]. However, these previous investigations have mainly focused on the mechanical behavior: the microstructural study is limited. It is vital to understand the changes in engineering properties that result from changes in the influential factors.

Models of the microstructure of fine-grained soils have been developed and modified since 1953 by geotechnical engineers to help understand soil behavior. Lambe's model is the first conceptual model, which considers clay particles to be single platelets.

* Corresponding author. Tel.: +66 44 22 4322, +66 89 767 5759; fax: +66 44 22 4607.
*E-mail addresses:* suksun@g.sut.ac.th, suksun@yahoo.com (S. Horpibulsuk), runglawa@gmail.com (R. Rachan), avirut@sut.ac.th (A. Chinkulkijniwat).

0950-0618/$ - see front matter © 2010 Elsevier Ltd. All rights reserved.
doi:10.1016/j.conbuildmat.2010.03.011

Since Lambe developed his theory, there have been significant improvements in microstructure observation techniques, leading towards complete description of the microstructure of fine-grained soils in relation to their engineering behavior such as the works reported by Gillott [21] and Collins and McGown [22]. Aylmore and Quirk [23]; Olsen [24]; and Nagaraj et al. [25] have revealed that the basic element of the microstructure of natural clay is not the single platelet but domains composed of various aggregated platelets.

Because cement and clay interacts with water, when clay is mixed with cement and water, clay and cement particles group together into large clay–cement clusters [26]. The cement gel is stable in the intra-aggregate and inter-aggregate pores because of the attractive forces (caused by physicochemical forces), and the capillary forces between the clay–cement clusters and the cement gel, respectively.

Abduljauwad [27] observed the microstructure changes of stabilized soils using scanning electron microscopes (SEMs). Keshawarz and Dutta [28] reported that the particles of uncemented soil appear as a blocky arrangement of loosely packed particles while the cemented soil has an abundance of tobermorite crystals. Previous works focusing on clay mineralogy [27,29–32] used X-ray diffraction techniques to investigate the mineralogical changes and to identify the reaction products formed when lime is added to clay soils.

Even though available researches exists on microstructure of cement-stabilized clay, they mainly focus on particular water content and curing time and do not cover all microstructural tests. This paper attempts to investigate the microstructural changes in cement-stabilized silty clay to explain the different strength development according to the influential factors, i.e., cement content, clay water content and curing time. Two sets of cemented samples were prepared for this study: samples with cement content $C = 0–10\%$ (practical range) and $C > 10\%$. In the first set, the investigation illustrates the role of the influential factors on the strength and microstructure development and determines the effective mixing state in the practical range. The second set is used to further understand the strength and microstructure development with cement to facilitate the determination of proper quantity of cement to be stabilized. The unconfined compressive strength was used as a practical indicator to investigate the strength development. The microstructural analyses were performed in this paper using a scanning electron microscope, mercury intrusion porosimetry, and thermal gravity tests.

**Table 1**
Chemical composition of ordinary Portland cement and silty clay.

| Chemical composition (%) | Portland cement | Silty clay |
|---|---|---|
| $SiO_2$ | 20.90 | 20.10 |
| $Al_2O_3$ | 4.76 | 7.55 |
| $Fe_2O_3$ | 3.41 | 32.89 |
| Cao | 65.41 | 26.15 |
| MgO | 1.25 | 0.47 |
| $SO_3$ | 2.71 | 4.92 |
| $Na_2O$ | 0.24 | ND |
| $K_2O$ | 0.35 | 3.17 |
| LOI | 0.96 | 3.44 |

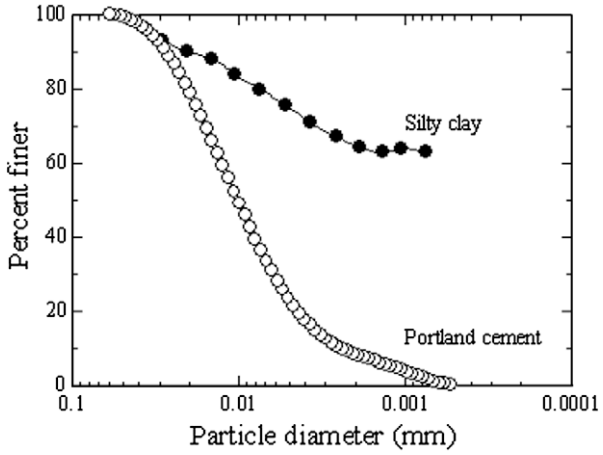


**Fig. 1.** Grain size distributions of Portland cement and silty clay.

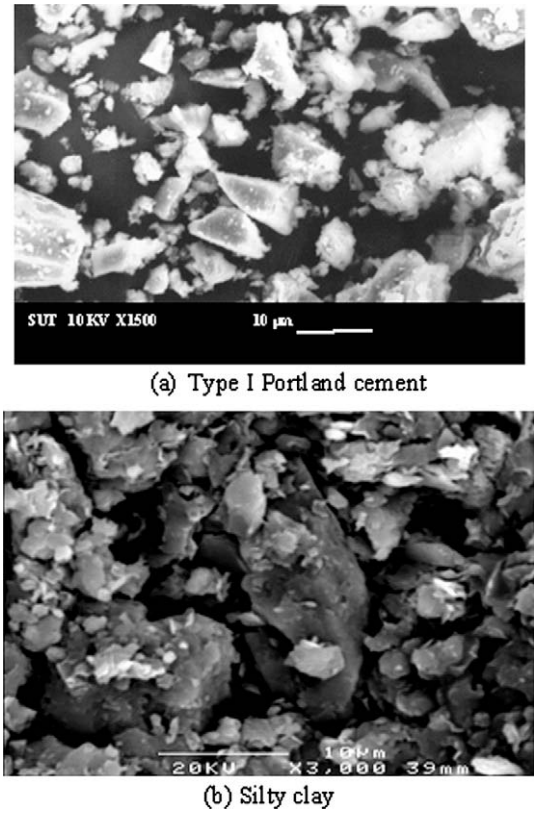


**Fig. 2.** SEM photos of cement and natural clay.

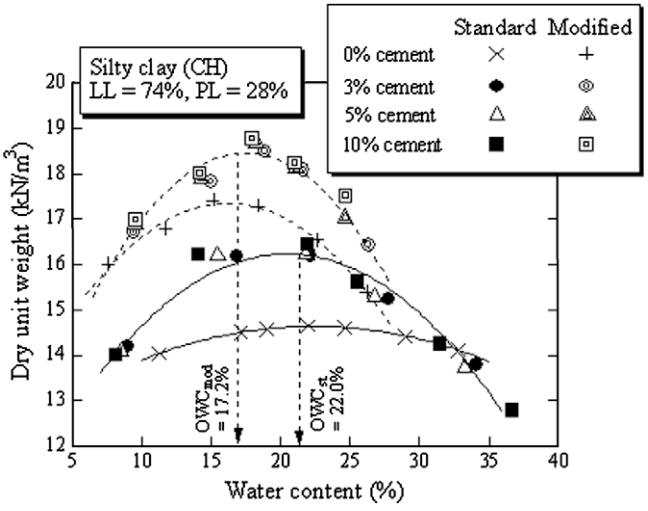


**Fig. 3.** Plot of dry unit weight versus water content of the uncemented and the cemented samples compacted under standard and modified Proctor energies.

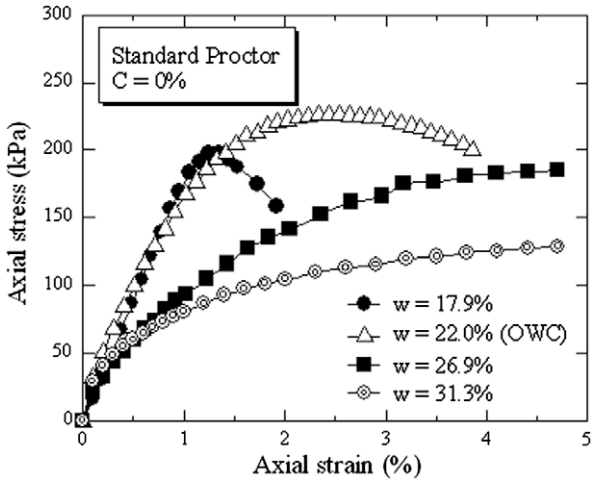


**Fig. 4.** Unconfined compression test result of compacted silty clay.

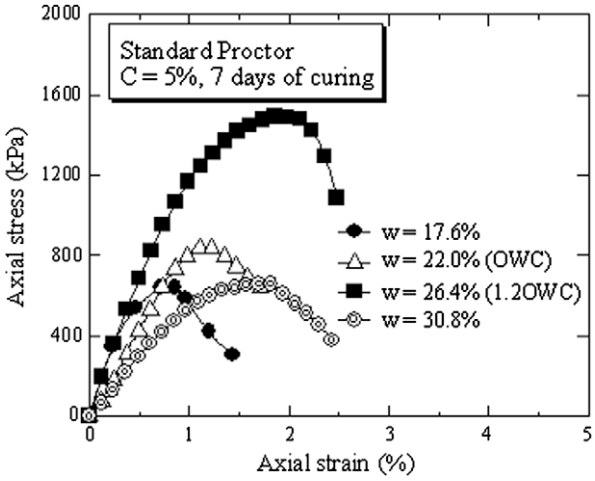


**Fig. 5.** Unconfined compression test result of the 5% cemented samples after 7 days of curing.

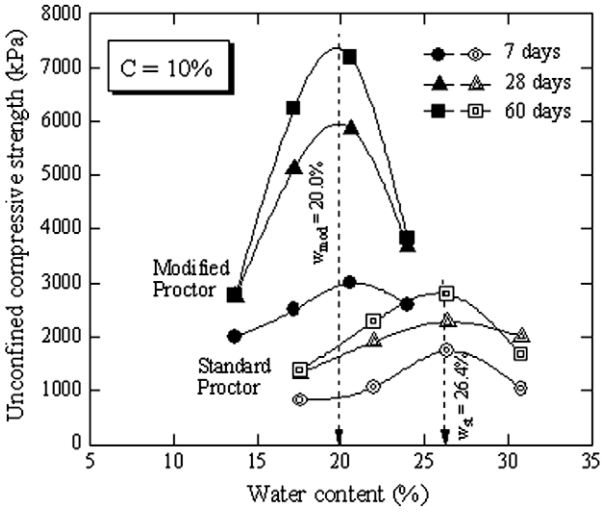


**Fig. 6.** Effect of compaction energy and curing time on strength development.

## 2. Laboratory investigation

The soil sample is silty clay collected from the Suranaree University of Technology campus in Nakhon Ratchasima, Thailand at a depth of 3 m. The soil is composed of 2% sand, 45% silt and 53% clay. Its specific gravity is 2.74. The liquid and plastic limits are approximately 74% and 27%, respectively. Based on the Unified Soil Classification System (USCS), the clay is classified as high plasticity (CH). During sampling, the groundwater had disappeared. The natural water content was 10 percent. The free swell test proposed by Prakash and Sridharan [33] shows that the clay is classified as low swelling with a free swell ratio (FSR) of 1.0. Ordinary (Type I) Portland cement with a specific gravity of 3.15 was used. The chemical composition and grain size distribution of the cement compared with those of the silty clay are shown in Table 1 and Fig. 1, respec-

**Table 2**
Basic properties of the cemented samples in the active zone.

| Cement (%) | Atterberg's limits (%) | | | *OWC* (%) | | $\gamma_{dmax}$ (kN/m$^3$) | |
|---|---|---|---|---|---|---|---|
| | LL | PL | PI | Std. | Mod. | Std. | Mod. |
| 0 | 74.1 | 27.5 | 46.6 | 22.4 | 17.2 | 14.6 | 17.4 |
| 3 | 74.1 | 45.0 | 29.1 | 22.2 | 17.5 | 16.2 | 18.5 |
| 5 | 72.5 | 45.0 | 27.5 | 21.8 | 17.3 | 16.2 | 18.7 |
| 10 | 71.0 | 44.8 | 26.2 | 22.0 | 17.4 | 16.4 | 18.8 |

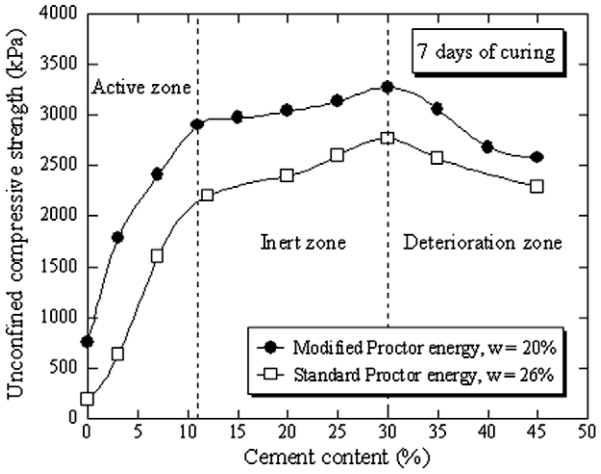


**Fig. 7.** Strength development as a function of cement content.

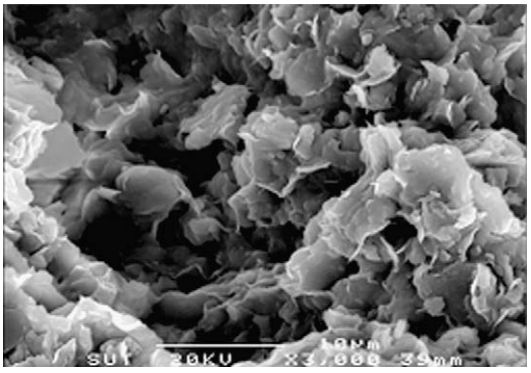

**Fig. 8.** SEM photo of the uncemented sample compacted at the *OWC* under the standard Proctor energy.

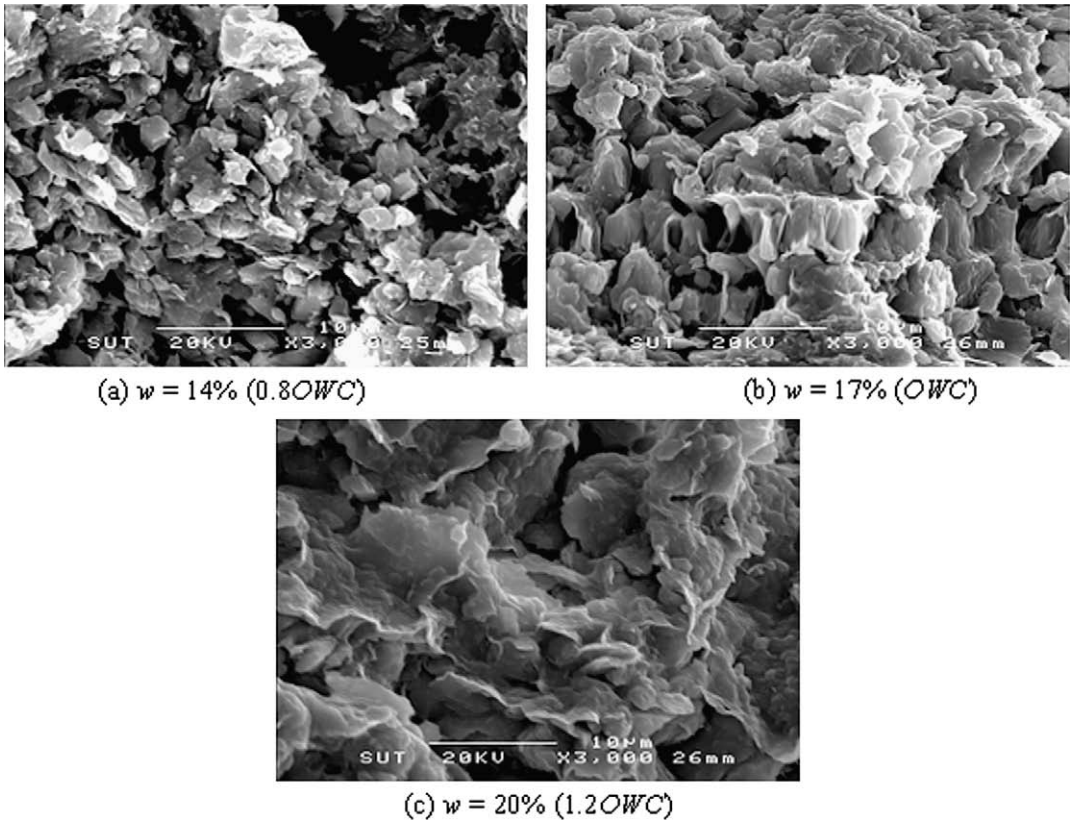


**Fig. 9.** SEM photos of the uncemented samples compacted at different molding water contents under modified Proctor energy.

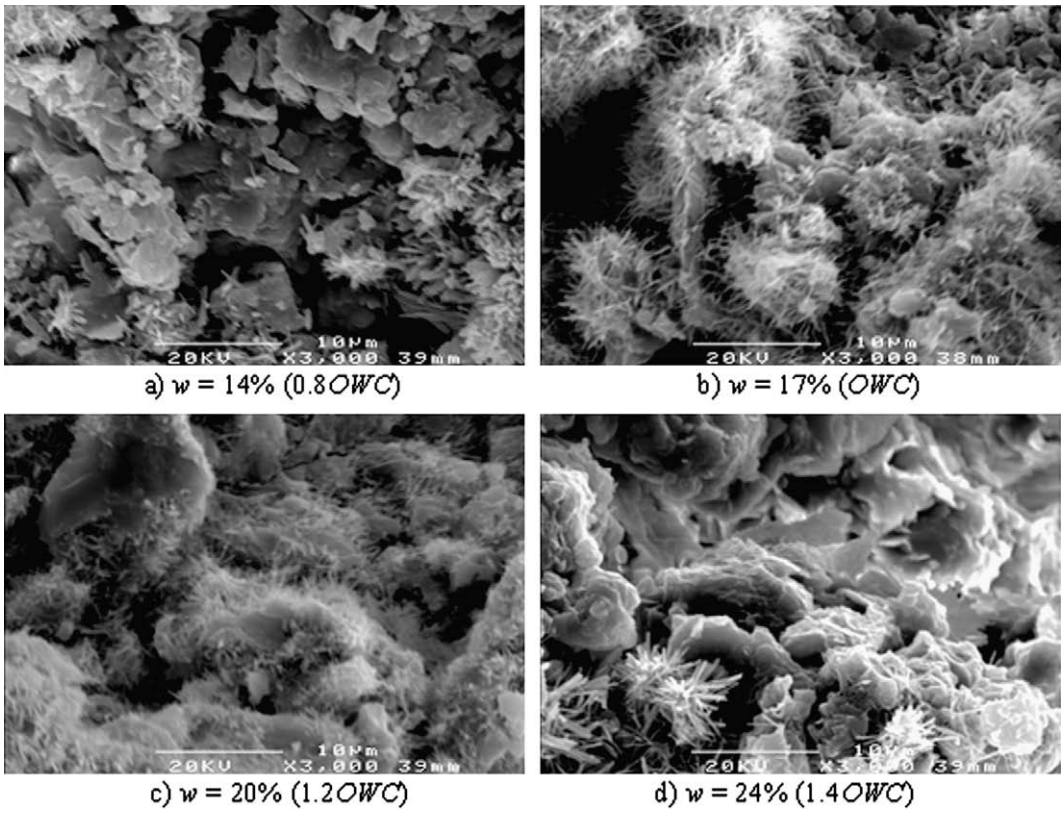


**Fig. 10.** SEM photos of the 10% cement samples compacted at different water contents under modified Proctor energy after 7 days of curing.

tively. The grain size distribution of the cement was obtained from laser particle size analysis. SEM photos of the cement and the natural silty clay are shown in Fig. 2. From the grain size distribution and the SEM photos, it is found that the particles of the silty clay are much smaller than those of the cement. The cement is irregular in shape, and the natural silty clay shows groups of cluster with various sizes.

The silty clay was passed through a 16-mm sieve to remove the coarser particles. It was air-dried for at least 3 days, and then the water content was adjusted for the compaction test. At least five compaction points were generated. The compaction was carried out according to ASTM D 698 and D 1557 in a standard 100-mm diameter mold for standard and modified Proctor energies (592.5 and 2693.3 kJ/m$^3$, respectively). The compaction characteristics (optimum water content, *OWC*, and maximum dry unit weight, $\gamma_{dmax}$) are 22.4% and 14.6 kN/m$^3$ for standard Proctor energy and 17.2% and 17.4 kN/m$^3$ for modified Proctor energy.

To investigate the role of cement content (in the practical range) on the index properties and compaction curve of the cemented clay, the clay–cement mixture was then thoroughly mixed with water specified for index and compaction tests in a soil mixer for 10 min as recommended by Miura et al. [13]. The total mixing and testing time was less than 40 min for both tests, which is less than the initial set time of the cement (about 2 h) [15].

For the strength test, having obtained the compaction curves of the base (uncemented) clay, the clay water content, *w*, was adjusted to 0.8, 1.0, 1.2 and 1.4 times the *OWC* for the first set of the cemented samples and adjusted to 1.2*OWC* for the second set of the cemented samples. In this study, the *OWC* of the base clay was used as a reference state for the stabilization. In practice, the *OWC* is very useful as the reference state for laboratory and field works because the *OWC* is intrinsic for a given clay and depends only on compaction energy. It is well recognized that the *OWC* of some clays compacted under various energies can be estimated from their index properties [34–36]. Recent works [36–38] have also revealed that the *OWC* at any compaction energy can be simply and rapidly approximated from the known *OWC* at a particular energy.

All the moist clay samples were mixed with cement and compacted in the standard mold. After 24 h, the cemented samples were removed from the molds, wrapped in vinyl bags and stored in a humidity chamber at a constant temperature (25 ± 2 °C). The unconfined compression test was run on the samples after 7, 28, and 60 days of curing. The rate of vertical displacement was fixed at 1 mm/min. For each curing time, compaction energy and combination of water content and cement content, at least three samples were tested under the same conditions to check for test consistency. In most cases, the results under the same testing condition were reproducible.

The cemented samples at the required water contents and curing times (7, 28, and 60 days) were carefully broken from the center into small fragments for the microstructural tests. SEM samples were frozen at −195 °C by immersion in liquid nitrogen for 5 min and evacuated at a pressure of 0.5 Pa at −40 °C for 5 days [39]. All samples were coated with gold before SEM (JOEL JSM-6400) analysis.

The pore size distribution was measured using a MIP with a pressure range from 0 to 288 MPa that is capable of measuring pore size diameters as small as 5.7 nm (0.0057 μm). A cubic sample with a volume of 1–2 cm$^3$ was used for testing. Hydration of the MIP samples was stopped by freezing and drying, as in the SEM examination preparation. Mercury porosimetry is expressed by the Washburn equation [40]. A constant contact angle ($\theta$) of 140° and a constant mercury surface tension ($\gamma$) of 480 dynes/cm were used for the pore size calculation.

Thermal gravity (TG) analysis is one of the widely accepted methods for determining the hydration products, which are crystalline $Ca(OH)_2$, calcium silicate hydrates (CSH), calcium aluminate hydrates (CAH), calcium aluminum silicate hydrates (CASH) and ettringite. The CSH, CAH, and CASH are regarded as cementitious products. The $Ca(OH)_2$ content was determined based on the weight loss between 450 and 580 °C [41,42] and expressed as a percentage by weight of the ignited sample. When heating the samples at temperatures between 450 and 580 °C, $Ca(OH)_2$ is decomposed into calcium oxide (CaO) and water, as in Eq. (1).

$$Ca(OH)_2 \rightarrow CaO + H_2O \quad (1)$$

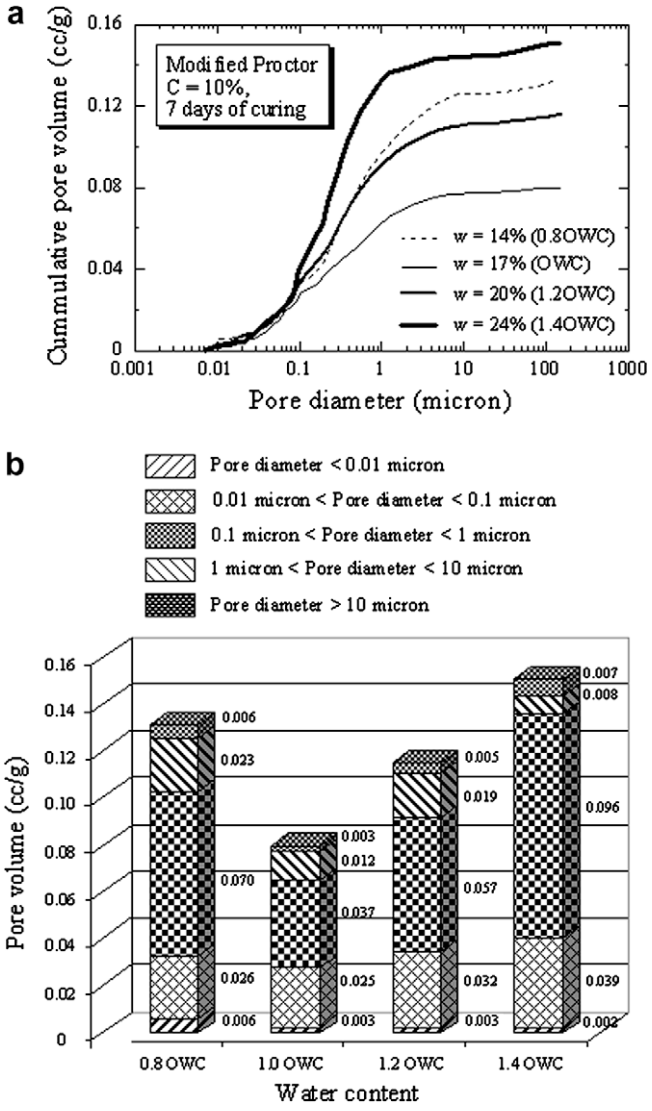


**Fig. 11.** Pore size distribution of the 10% cement samples compacted at different water contents under modified Proctor energy after 7 days of curing.

**Table 3**
$Ca(OH)_2$ of the 10% cement samples compacted at different water contents under modified Proctor energy after 7 days of curing.

| Water content (%) | Weight loss (%) | $Ca(OH)_2$ (%) |
|---|---|---|
| 14% (0.8*OWC*) | 1.42 | 5.84 |
| 17% (*OWC*) | 1.46 | 6.00 |
| 20% (1.2*OWC*) | 1.52 | 6.25 |
| 24% (1.4*OWC*) | 1.40 | 5.75 |

Because of the heat, the water is lost, which decreases the overall weight. The amount of $Ca(OH)_2$ can be approximated from this lost water by Eq. (1), which is 4.11 times the amount of lost water [41]. The change in the cementitious products can be expressed by the change in $Ca(OH)_2$ because they are the hydration products. Prior to TG testing, the hydrated samples were ground in a ball mill and sieved through a 100-mesh (150 μm). Approximately 10–20 mg of the sample was taken for the analysis. All samples were heated up to 1000 °C at a rate of 10 °C/min.

## 3. Compaction and unconfined compression test results

Compaction and strength test results for samples with $C = 0$ to 10% are shown in Figs. 3–6. Fig. 3 shows the plots of dry unit weight versus molding water content of the uncemented and the cemented samples compacted under the standard and modified Proctor energies. It is noted that the maximum dry unit weight of the cemented samples is higher than that of the uncemented samples whereas their optimum water content is practically the same. This characteristic is the same as that of cement stabilized coarse-grained soils as reported by Horpibulsuk et al. [19]. The adsorption of $Ca^{2+}$ ions onto the clay particle surface decreases the repulsion between successive diffused double layers and increases edge-to-face contacts between successive clay sheets [43,44]. Thus, clay particles flocculate into larger clusters, which increases in the plastic limit with an insignificant change in the liquid limit (*vide* Table 2). As such, the plasticity index of the mixture results from the significant increase in the plastic limit. This finding is consistent with the test results of the cement-stabilized Bangkok clay reported by Uddin [9], which is also classified as a low swelling clay [45]. Because the *OWC* of low swelling clays is mainly controlled by the liquid limit [35,36], the *OWC*s of the uncemented and the cemented samples are almost the same (*vide* Table 2).

Typical stress and strain relationships of the uncemented and cemented samples for different water contents are shown in Figs. 4 and 5. It is noted that the strength and stiffness of the uncemented samples increase with water content up to the optimum water content (densest package) and decrease when the water content is on the wet side of optimum. This characteristic is different from that of the cemented samples in which the maximum strength and stiffness are at 1.2*OWC*.

The role of curing time and compaction energy on the strength development of the cemented clay is illustrated in Fig. 6. It is shown that at a particular curing time, the strength curve depends on the compaction energy. As the compaction energy increases, the maximum strength increases and the water content at maximum strength decreases. For the same compaction energy, the strength curves follow the same pattern for all curing times, which are almost symmetrical around 1.2*OWC* for the range of the water content tested.

The role of cement content in the strength development at a particular water content is now examined. Fig. 7 shows the strength development with cement content (varied over a wide range) of the cemented samples compacted under the modified

**Table 4**
$Ca(OH)_2$ of the 10% cement samples compacted at 1.2*OWC* under modified Proctor energy at different curing times.

| Curing time (days) | Weight loss (%) | $Ca(OH)_2$ (%) |
|---|---|---|
| 7 | 1.52 | 6.25 |
| 28 | 1.65 | 6.78 |
| 60 | 1.85 | 7.63 |

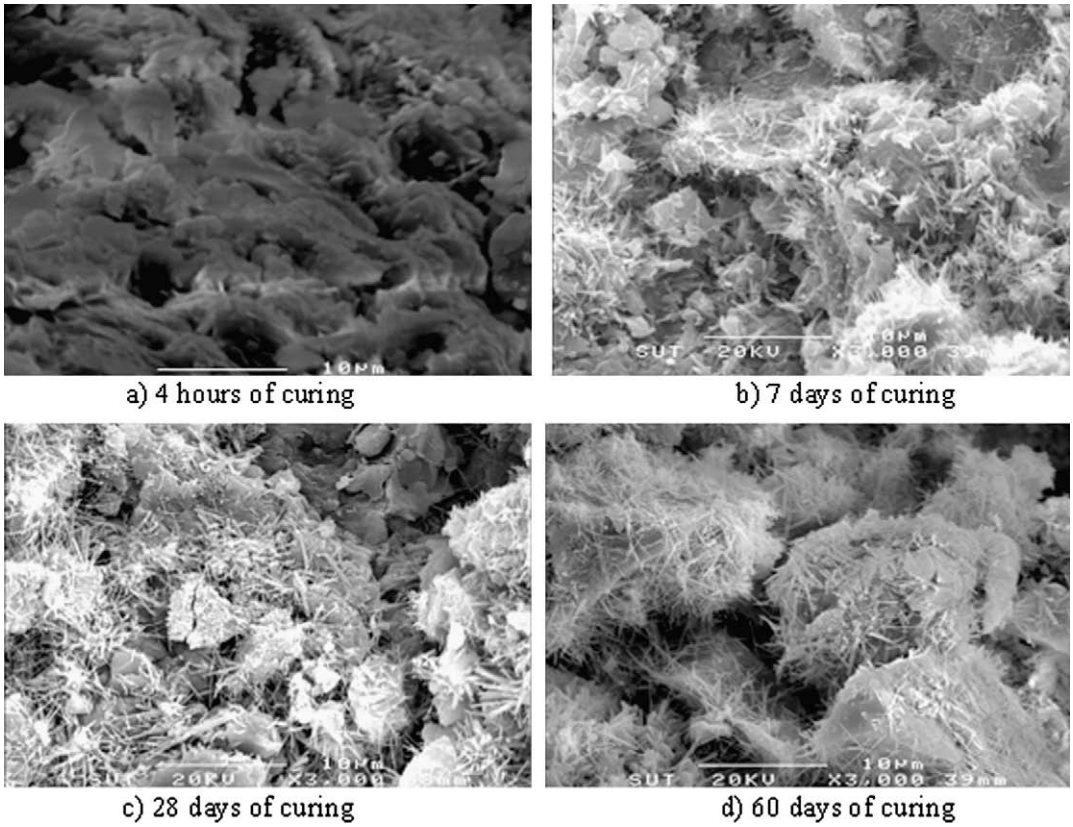


**Fig. 12.** SEM photos of the 10% cement samples compacted at 1.2*OWC* under modified Proctor energy at different curing times.

Proctor energy at 1.2*OWC* (20%) after 7 days of curing. The strength increase can be classified into three zones. As the cement content increases, the cement per grain contact point increases and, upon hardening, imparts a commensurate amount of bonding at the contact points. This zone is designated as the *active zone*. Beyond this zone, the strength development slows down while still gradually increasing. The incremental gradient becomes nearly zero and does not make any further significant improvement. This zone is referred to as the *inert zone* ($C$ = 11–30%). The strength decrease appears when $C$ > 30%. This zone is identified as the *deterioration* zone. From all the test results, it is concluded that $C$ < 11% is the active zone in which the optimal water content (effective mixing state) is 1.2*OWC* for all the compaction energies and curing times, regardless of cement content. The same is not true for $C$ > 11%: the optimal water content depends on cement content. As such, the improvement zone proposed is valid only for $w$ = 1.2*OWC*.

## 4. Microstructural analysis

### 4.1. Uncemented samples

For compacted fine-grained soils, the soil structure mainly controls the strength and resistance to deformation, which is governed by compaction energy and water content. Compaction breaks down the large clay clusters into smaller clusters and reduces the pore space (*vide* Figs. 2b and 8). Fig. 9 shows SEM photos of the uncemented samples compacted under the modified Proctor energy at water contents in the range of 0.8–1.2*OWC*. On the wet side of optimum (*vide* Fig. 9c), a dispersed structure is likely to develop because the quantity of pore water is enough to develop a complete double layer of the ions that are attracted to the clay particles. As such, the clay particles and clay clusters easily slide over each other when sheared, which causes low strength and stiffness. On the dry side of optimum (*vide* Fig. 9a), there is not sufficient water to develop a complete double layer; thus, the distance between two clay platelets is small enough for van der Waals type attraction to dominate. Such an attraction leads to flocculation with more surface to edge bonds; thus, more aggregates of platelets lead to compressible flocs, which make up the overall structure. At the *OWC*, the structure results from a combination of these two characteristics. Under this condition, the compacted sample exhibits the highest strength and stiffness. The role of compaction energy is clearly shown in Figs. 8 and 9b. More aggregates are seen for the modified Proctor energy.

### 4.2. Cemented samples

#### 4.2.1. Effect of water content

Fig. 10 shows SEM photos of the 10% cement samples compacted at different water contents under the modified Proctor energy and cured for 7 days. It is clearly seen that the pores are filled with hydration products (well-knitted framework), especially for the samples with $w$ = 17% (*OWC*) and 20% (1.2*OWC*). The samples with $w$ = 14% (0.8*OWC*) and 24% (1.4*OWC*) show fewer hydration products. Water content influences not only the hydration products but also the pore volume, especially for 1.0–0.1 μm pores, which have the highest volume (*vide* Fig. 11). The microstructural change with water content in the cemented samples is similar to that of the uncemented samples. The densest state (lowest total pore volume) is at the optimum water content. The looser states (larger total pore volume) are found on the dry and the wet sides of optimum. Larger total pore volume is associated with larger 1.0–0.1 μm pore volume.

Even though the total pore volume of the sample for $w$ = 17% (*OWC*) is the lowest (Fig. 11), the strength is not the highest. This implies that, for the cemented samples, in addition to the fabric, the cementation bond controls the strength development. The sample for $w$ = 21% (1.2*OWC*) exhibits the highest strength because it contains the highest amount of cementitious products, as shown by the highest amount of $Ca(OH)_2$ (Table 3). Thus, in the active zone where $C$ < 11%, 1.2*OWC* is optimal for cement stabilization.

#### 4.2.2. Effect of curing time

Fig. 12 shows SEM photos of the 10% cement samples compacted at $w$ = 20% (1.2*OWC*) under the modified Proctor energy and cured for different curing times. After 4 h of curing, the soil clusters and the pores are covered and filled by the cement gel (hydrated cement) (*vide* Fig. 12a). Over time, the hydration products in the pores are clearly seen and the soil–cement clusters tend to be larger (*vide* Fig. 12b–d) because of the growth of cementitious products over time (*vide* Table 4).

The effect of curing time on the pore size distribution of the cemented samples is illustrated in Fig. 13. It is found that, during the early stage of hydration (fewer than 7 days of curing), the volume of pores smaller than 0.1 μm significantly decreases while the volume of pores larger than 0.1 μm slightly increases. This result shows that, during 7 days of curing, the cementitious products fill

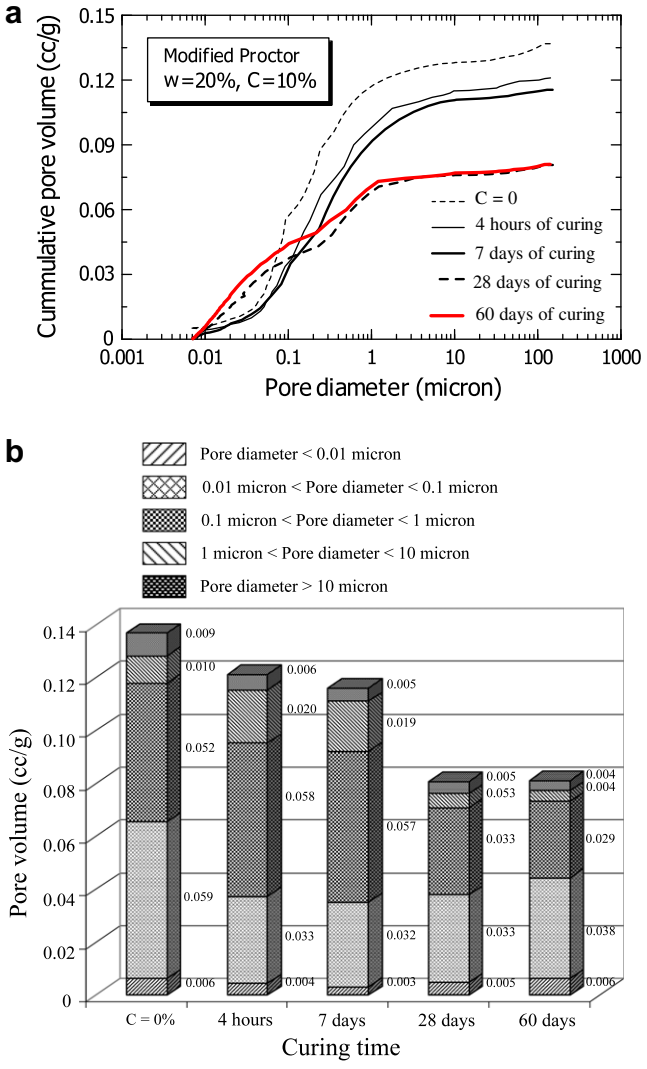


**Fig. 13.** Pore size distribution of the 10% cement samples compacted at 1.2*OWC* under modified Proctor energy at different curing times.

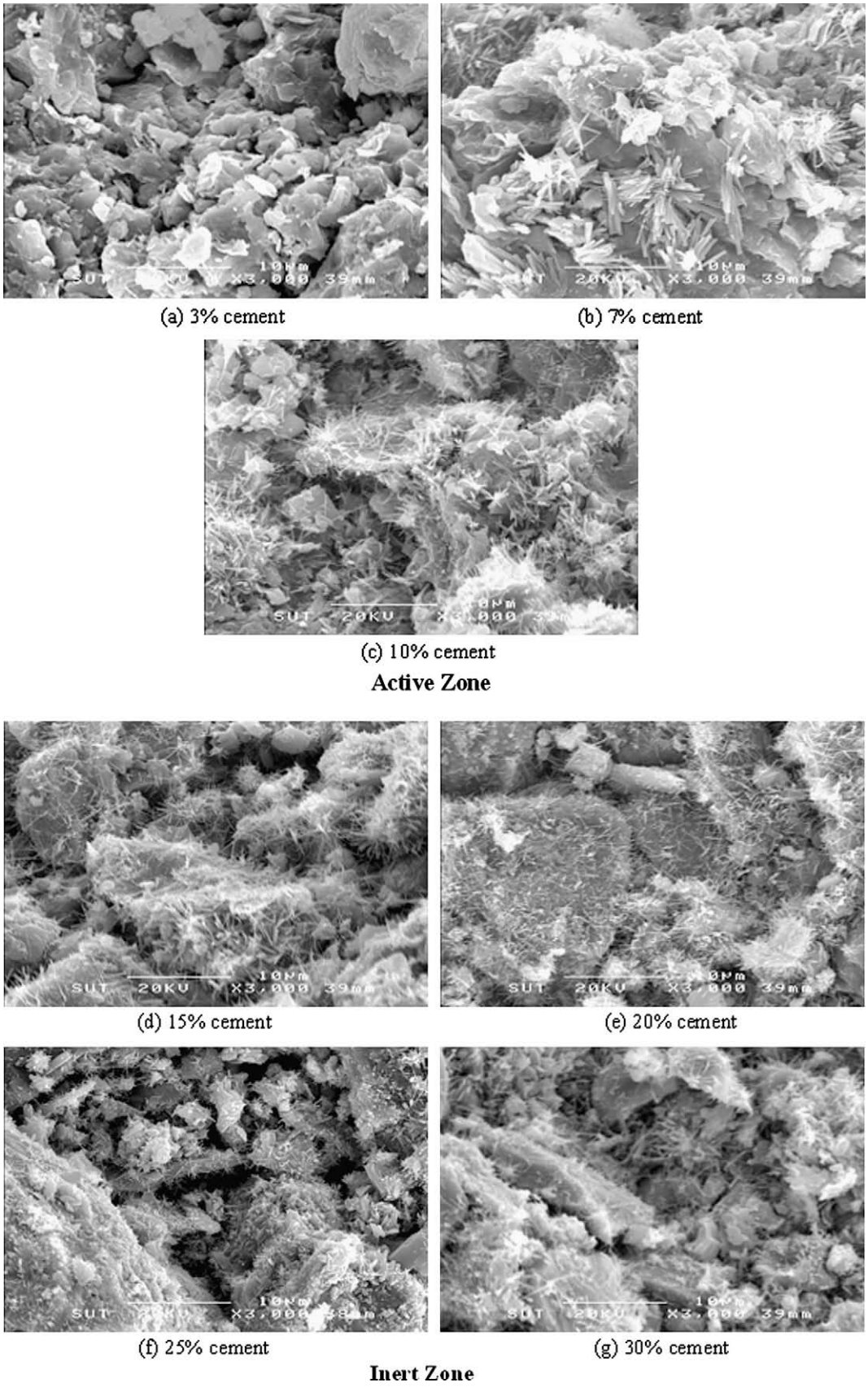


**Fig. 14.** SEM photos of the cemented samples compacted at different cement contents under modified Proctor energy after 7 days of curing.

pores smaller than 0.1 μm and the coarse particles (unhydrated cement particles) cause large soil–cement clusters and large pore space. After 7 days of curing, the volume of pores larger than 0.1 μm tends to decrease while the volume of pores smaller than 0.1 μm tends to increase possibly because the cementitious products fill the large pores (larger than 0.1 μm). As a result, the volume

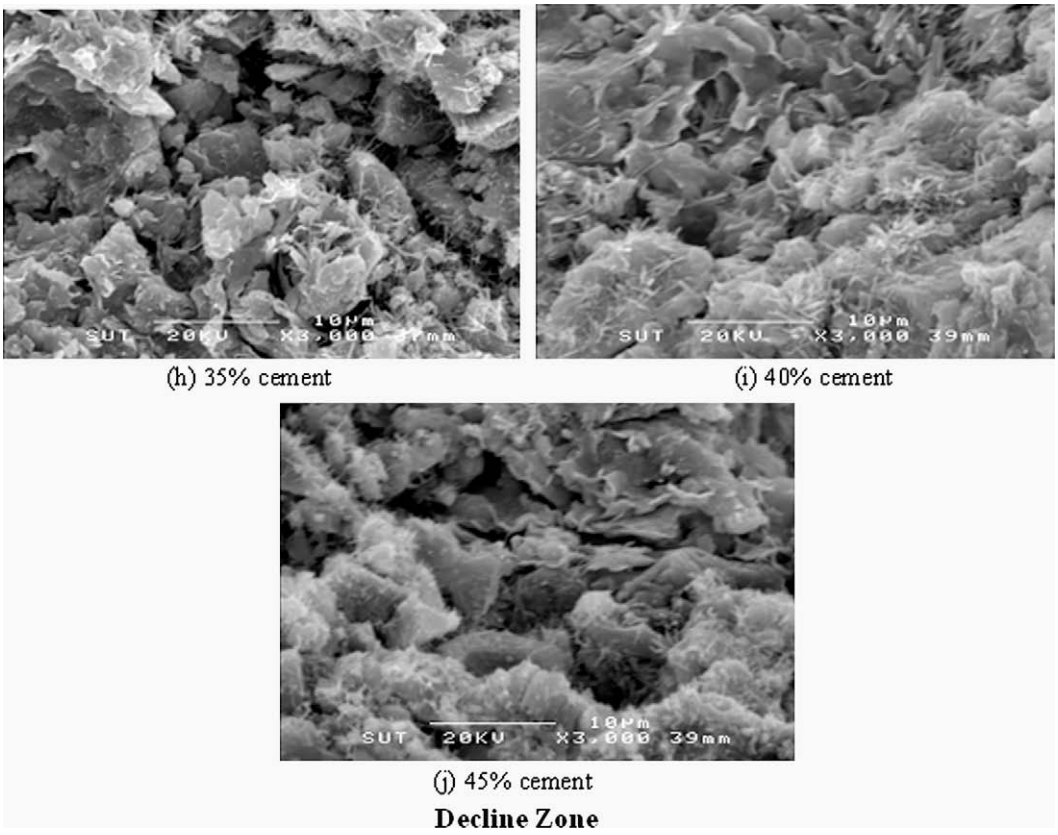


**Fig. 14** (*continued*)

of small pores (smaller than 0.1 μm) increases, and the total pore volume decreases.

*4.2.3. Effect of cement content*

This study focuses on understanding the microstructure development with cement content for a particular water content. Figs. 14 and 15 and Table 5 show the SEM photos, pore size distribution, and the amount of $Ca(OH)_2$ of the cemented samples compacted at $w = 20\%$ under the modified Proctor energy for different cement contents after 7 days of curing. Fig. 14a–c, d–g, and h–j shows SEM photos of the cemented samples in the active, inert, and deterioration zones, respectively. The SEM photo of the 3% cement sample (Fig. 14a) is similar to that of the uncemented sample because the input of cement is insignificant compared to the soil mass. As the cement content increases in the active zone, hydration products are clearly seen in the pores (*vide* Fig. 14b and c) and the cementitious products significantly increase (Table 5). The cementitious products not only enhance the inter-cluster bonding strength but also fill the pore space, as shown in Fig. 15: the volume of pores smaller than 0.1 μm is significantly reduced with cement, thus, the reduction in total pore volume. As a result, the strength significantly increases with cement. For the inert zone, the presence of hydration products (Fig. 14d–g) and cementitious products (Table 5) is almost the same for 15–30% cement. This results in an insignificant change in the pore size distribution and, thus, the strength. For the deterioration zone (Fig. 14h–j), few hydration products are detected. Both the volumes of the highest pore size interval (1.0–0.1 μm pores) and the total pore tend to increase with cement (Fig. 15). This is because the increase in cement content significantly reduces the water content, which decreases the degree of hydration and, thus, cementitious products (Table 5). To improve the strength in this zone, higher clay water content is required. The optimal clay water content for this zone is however not studied in this paper because this range of cement content is far from the practical range (active zone). It is concluded from this study that for a particular water content, the input of cement in excess of the active zone is useless.

## 5. Discussion

Based on the cluster theory [25,32], the pores are classified into two categories: inter-aggregate pores (larger than 0.01 μm) and intra-aggregate pores (smaller than 0.01 μm). After mixing clay with cement, the formation of clay–cement clusters due to physico-chemical interaction reduces the small inter-aggregate pore (0.01–0.1 μm) volume and slightly increases the large inter-aggregate pore (0.1–10 μm) volume, resulting in the increase in the dry unit weight. Because of the growth of cementitious products with time, large inter-aggregate pores are filled, and thus, the total pore volume decreases.

From this investigation, it is found that for the active zone, $w = 1.2OWC$ is the effective mixing state. Beyond this water content, the strength decreases because of the decrease in the clay–water/cement ratio, $w_c/C$ [13–15,18,19]. The effective mixing state ($1.2OWC$) for the cemented clays can be attained simply by the rapid method of estimating the compaction curves and by the Modified Ohio's compaction curves [36,38]. The relationship between $OWC/OWC_{st}$ and compaction energy for various soils is unique and is expressed in the form:

$$\frac{OWC}{OWC_{st}} = 2.02 - 0.37 \log E \tag{2}$$

where $E$ is in the range of 296.3–2693.3 kJ/m$^3$ and $OWC_{st}$ is the optimum water content at the standard Proctor energy. From this equa-

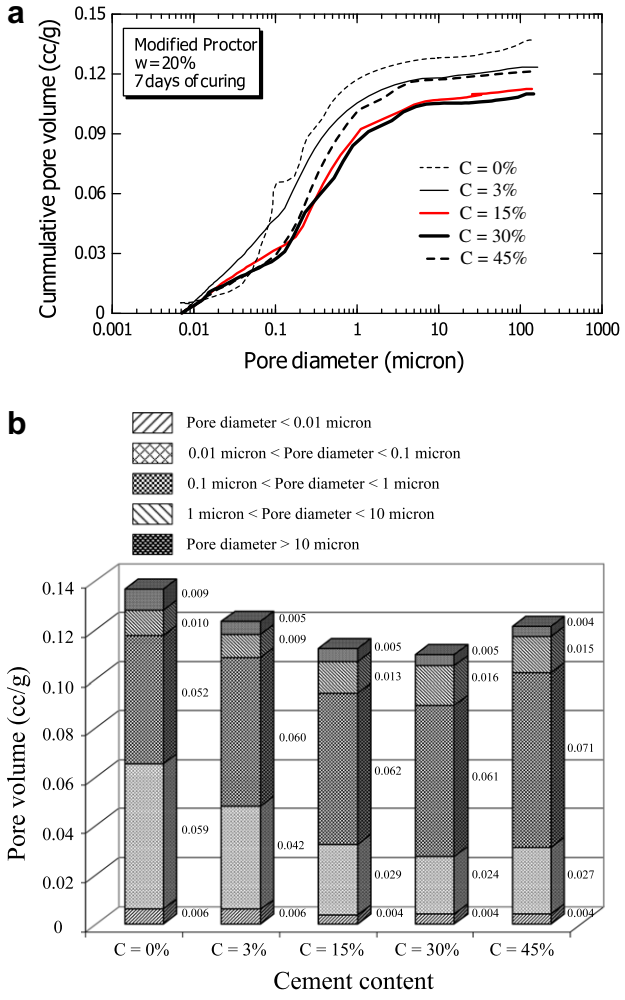


**Fig. 15.** Pore size distribution of the cemented samples compacted at different cement contents under modified Proctor energy after 7 days of curing.

**Table 5**
$Ca(OH)_2$ of the cemented samples compacted at different cement contents under modified Proctor energy after 7 days of curing.

| Improvement zones | Cement (%) | Weight loss (%) | $Ca(OH)_2$ (%) |
|---|---|---|---|
| Active | 3 | 1.34 | 5.51 |
| | 7 | 1.50 | 6.17 |
| | 11 | 1.60 | 6.58 |
| Inert | 15 | 1.62 | 6.66 |
| | 20 | 1.65 | 6.78 |
| | 30 | 1.68 | 6.90 |
| Deterioration | 35 | 1.54 | 6.33 |
| | 40 | 1.48 | 6.08 |
| | 45 | 1.37 | 5.63 |

tion, *OWC* at any compaction energy can be estimated from the known $OWC_{st}$. This is an advantage of the study using the compaction characteristics of the uncemented clay as the reference state.

## 6. Conclusions

This paper analyzes strength development considering soil microstructure using a scanning electron microscope, mercury intrusion pore size distribution measurements, and thermal gravity analysis. The following conclusions can be advanced from this study.

1. The strength development with cement content for a specific water content is classified into three zones: active, inert and deterioration. In the active zone, the volume of pores smaller than 0.1 μm significantly decreases with the addition of cement because of the increase in cementitious products. In the inert zone, both pore size distribution and cementitious products change insignificantly with increasing cement; thus, there is a slight change in strength. In the deterioration zone, the water is not adequate for hydration because of the excess of cement input. Consequently, as cement content increases, the cementitious products and strength decreases.
2. In the active zone, the maximum strength of the cemented clay (effective mixing state) is at a water content that is 1.2 times the optimum water content. Under this condition, the inter-cluster cementation bonding strength is strongest, even though the total pore volume is higher than that at the optimum water content. This implies that both fabric and cementation bonds control strength development.
3. In the active zone, the effective mixing state is introduced in terms of the optimum water content of the base clay. It is very useful in practice because the *OWC* of a clay is intrinsic and depends only on the compaction energy. The *OWC* for any compaction energy can be rapidly approximated using the Modified Ohio's compaction curves.
4. At the initial stage of stabilization, the volume of small pores (smaller than 0.1 μm) significantly decreases while the volume of large pores (larger than 0.1 μm) increases with increasing cement. The increase in volume of the large pores is induced by the unhydrated cement particles. After 7 days of curing, the large pore volume and total pore volume decrease while the volume of the small pores increases. This is because of the growth of the cementitious products that fill the large pores.

## Acknowledgements

The authors would like to acknowledge the financial support provided by theCommission on Higher Education (CHE) and the Thailand Research Fund (TRF) under the contract MRG5080127. Facilities, equipments and financial support provided by the Suranaree University of Technology are appreciated. The technical comments by Prof. T.S. Nagaraj (now deceased), Indian Institute of Science, as well as those by Dr. Amnat Apichatvullop and Dr. Theerawat Sinsiri, Suranaree University of Technology, are appreciated.

## References

[1] Horpibulsuk S, Kumpala A, Katkan W. A case history on underpinning for a distressed building on hard residual soil underneath non-uniform loose sand. Soils and Found 2008;48(2):267–86.
[2] Kohgo Y, Tamrakar SB, Tang HG. Investigations on the mechanical properties of typical soils distributed in northeast Thailand for the construction of irrigation facility. Technical Report, Japan International Research Center for Agricultural Sciences; 1970. p. 222.
[3] Kohgo Y, Horpibulsuk S. Simulation of volume change behavior of yellow soil sampled from Khon Kaen City in Northeast Thailand. In: Proceedings of the 11th Asian regional conference on soil mechanics and geotechnical engineering, Soul, Korea, 1999. p. 141–4.
[4] Udomchore V. Origin and engineering characteristics of the problem soils in the Khorat Basin. Northeastern Thailand, D.Tech. Dissertation, Asian Institute of Technology; 1991.
[5] Terashi M, Tanaka H, Okumura T. Engineering properties of lime treated marine soils and DMM. In: Proceedings of the 6th Asian regional conference on soil mechanics and foundation engineering; 1979. p. 191–4.
[6] Kawasaki T, Niina A, Saitoh S, Suzuki Y, Honjo Y. Deep mixing method using cement hardening agent. In: Proceedings of the 10th international conference on soil mechanics and foundation engineering; 1981. p. 721–4.
[7] Clough GW, Sitar N, Bachus RC, Rad NS. Cemented sands under static loading. J Geotechn Eng Div, ASCE 1981;107(GT6):799–817.
[8] Kamon M, Bergado DT. Ground improvement techniques. In: Proceedings of the 9th Asian regional conference on soil mechanics and foundation engineering; 1992. p. 526–46.

[9] Uddin K. Strength and deformation behaviour of cement treated Bangkok clay. Doctoral Thesis, Asian Institute of Technology, Bangkok, Thailand; 1994.
[10] Yin JH, Lai CK. Strength and stiffness of Hong Kong marine deposit mixed with cement. Geotechn Eng J 1998;29(1):29–44.
[11] Consoli NC, Rotta GV, Prietto PDM. Influence of curing under stress on the triaxial response of cemented soil. Geotechnique 2000;50(1):99–105.
[12] Kasama K, Ochiai H, Yasufuku N. On the stress–strain behaviour of lightly cemented clay based on an extended critical state concept. Soils Found 2000;40(5):37–47.
[13] Miura N, Horpibulsuk S, Nagaraj TS. Engineering behavior of cement stabilized clay at high water content. Soils Found 2001;41(5):33–45.
[14] Horpibulsuk S, Miura N. A new approach for studying behavior of cement stabilized clays. In: Proceedings of the 15th international conference on soil mechanics and geotechnical engineering (ISSMGE), Istanbul, Turkey; 2001. p. 1759–62.
[15] Horpibulsuk S, Miura N, Nagaraj TS. Assessment of strength development in cement-admixed high water content clays with Abrams' law as a basis. Geotechnique 2003;53(4):439–44.
[16] Horpibulsuk S, Bergado DT, Lorenzo GA. Compressibility of cement admixed clays at high water content. Geotechnique 2004;54(2):151–4.
[17] Horpibulsuk S, Miura N, Bergado DT. Undrained shear behavior of cement admixed clay at high water content. J Geotechn Geoenviron Eng, ASCE 2004;30(10):1096–105.
[18] Horpibulsuk S, Miura N, Nagaraj TS. Clay–water/cement ratio identity of cement admixed soft clay. J Geotechn Geoenviron Eng, ASCE 2005;131(2):187–92.
[19] Horpibulsuk S, Katkan W, Sirilerdwattana W, Rachan R. Strength development in cement stabilized low plasticity and coarse grained soils: laboratory and field study. Soils Found 2006;46(3):351–66.
[20] Horpibulsuk S, Liu MD, Liyanapathirana DS, Suebsuk J. Behavior of cemented clay simulated via the theoretical framework of the Structured Cam Clay model. Comput Geotechn 2010;37:1–9.
[21] Gillott JE. Fabric of Leda clay investigated by optical, electron-optical, and X-ray diffraction methods. Eng Geol 1970;4(2):133–53.
[22] Collins K, McGown A. The form and function of microfabric features in a variety of natural soils. Geotechnique 1974;24:233–54.
[23] Aylmore LAG, Quirk JP. Domain or turbostratic structure of clays. Nature 1960;187:1046.
[24] Olsen HW. Hydraulic flow through saturated clays. Clays Clay Miner 1962;9(2):131–61.
[25] Nagaraj TS, Vatasala A, Srinivasa Murthy BR. Discussion on "Change in pore size distribution due to consolidation of clays" by F.J. Griffith and R.C. Joshi. Geotechnique 1990;40(2):303–5.
[26] Horpibulsuk S, Rachan R, Raksachon Y. Role of fly ash on strength and microstructure development in blended cement stabilized silty clay. Soils Found 2009;49(1):85–98.
[27] Abduljauwad SN. Improvement of plasticity and swell potential of calcareous expansive clays. Geotechn Eng J 1995;26(1):3–16.
[28] Keshawarz MS, Dutta U. Stabilization of South Texas soils with fly ash. In: Proceedings of the geotechnical special publication no. 36, ASCE; 1993.
[29] Eades JL, Grim RE. Reaction of hydrated lime with pure clay minerals in soil stabilization. Highway Res Board 1960;262:51–63.
[30] Willoughby DR, Gross KA, Ingles OG, Silva SR, Spiers VM. The identification of reaction products in alkali stabilized clays by electron microscopy X-ray and electron diffraction. In: Proceedings of the 4th conference of the Australian road research board; 1968. p. 1386–408.
[31] Lambe TW, Whitman RV. The role of effective stress in the behavior of expansive soils. Quart Colo School Mines 1959;54(4):33–66.
[32] Mitchell JK. Fundamentals of soil behavior. John Wiley & Sons, Inc.; 1976. p. 422.
[33] Prakash K, Sridharan A. Free swell ratio and clay mineralogy of fine-grained soils. Geotechn Test J, ASTM 2004;27(2):220–5.
[34] Gurtug Y, Sridharan A. Compaction behaviour and prediction of its characteristics of fine grained soils with particular reference to compaction energy. Soils Found 2004;44(5):27–36.
[35] Nagaraj TS, Lutenegger AJ, Pandian NS, Manoj M. Rapid estimation of compaction parameters for field control. Geotechn Test J, ASTM 2006;29(6):1–10.
[36] Horpibulsuk S, Katkan W, Apichatvullop A. An approach for assessment of compaction curves of fine-grained soils at various energies using a one point test. Soils Foundations 2008;48(1):115–25.
[37] Blotz LR, Benson C, Boutwell G. Estimating optimum water content and maximum dry unit weight for compacted clays. J Geotechn Eng, ASCE 1998;124(9):907–12.
[38] Horpibulsuk S, Katkan W, Naramitkornburee A. Modified Ohio's curves: a rapid estimation of compaction curves for coarse- and fine-grained soils. Geotechn Test J, ASTM 2009;32(1):64–75.
[39] Chindaprasirt P, Jaturapitakkul C, Sinsiri T. Effect of fly ash fineness on compressive strength and pore size of blended cement paste. Cem Concr Compos 2005;27:425–8.
[40] Washburn EW. Note on method of determining the distribution of pore size in porous material. Proc Natl Acad Sci USA 1921:115–6.
[41] El-Jazairi B, Illston JM. The hydration of cement plate using the semi-isothermal method of thermogravimetry. Cem Concr Res 1980;10:361–6.
[42] Wang KS, Lin KL, Lee TY, Tzeng BY. The hydration characteristics when $C_2S$ is present in MSWI fly ash slag. Cem Concr Res 2004;26:323–30.
[43] Locat J, Berube MA, Choyuette M. Laboratory investigations on the lime stabilization of sensitive clay: shear strength development. Can Geotechn J 1990;27:294–304.
[44] Chew SH, Kamaruzzaman AHM, Lee FH. Physicochemical and engineering behavior of cement treated clays. J Geotechn Geoenviron Eng, ASCE 2004;130(7):696–706.
[45] Horpibulsuk S, Shibuya S, Fuenkajorn K, Katkan W. Assessment of engineering properties of Bangkok clay. Can Geotechn J 2007;44(2):173–87.